14

Parallel Computation of Large Neuronal Networks with Structured Connectivity

Marconi Barbosa[1], Karl Dockendorf[2], Miguel Escalona[3], and Borja Ibarz[4]
Aris Miliotis[2], Irene Sendiña-Nadal[4], Gorka Zamora-López[5]
and Lucia Zemanová[5]

[1] University of São Paulo, Brazil
marconi@if.sc.usp.br
[2] University of Florida, USA
am397@ufl.edu
[3] Universidad de Los Andes, Venezuela
angele@ula.ve
[4] Universidad Rey Juan Carlos, Spain
borja.ibarz@urjc.es
[5] University of Potsdam, Germany
gorka@agnld.uni-potsdam.de

14.1 Introduction

One does not need to delve into complex modern physical phenomena to realize that laws of physical nature are vastly employed and exploited by nature. We can see in an object as ubiquitous as a flower, among other striking properties related to its form, that the anther is isolated and the stigma is grounded, readily providing an electrostatic mechanism for charged bees to carry the pollen [1]. This phenomenon is so basic, yet shows what years of evolution manage with one charged particle, its surplus and absence.

The quest to understand and somehow control biological systems, using fundamentals and even by-products from physics and mathematics, has a long history. Only to mention a very few examples and recent observations: an original model of rhythmic waves coordinated by a central pattern generator in multi-legged animal locomotion [2, 3], models dealing with the mechanism of pattern formation (a perspective in [4]); a description of the formation of sunflowers' spirals and their relationship to Fibonacci series [5]; and new phenomena and nonlinear mechanical models of hearing [6, 7]. Most of these works require multidisciplinary thinking and address a larger community at various levels of mathematical sophistication, see [8] for a recent selection of biologically related material.

Among biological systems in general, the mammalian nervous system is arguably the richest example of the interplay between biology, physics, chemistry

and geometry. In the brain, vastly complex physical phenomena occur, but not only because of the raw number of interacting units and their hierarchical organization. The units themselves [9–12] as well as their effective connectivity [13–15] are still a major challenge to comprehension.

Various reports attempting to model aspects of neuronal activity with tools from nonlinear dynamics have aroused a growing acceptance of the fact that the diverse biological reactions of a cell to a stimulus can be explained by bifurcation theory. While many types of receptors and channels (which need to be taken into account in a description of the cell's intrinsic properties) might be present in a specific cell, they only determine the type of bifurcation of the neural dynamical behavior [16].

Of more interest to us is the thriving activity in modeling networks of neurons with diverse levels of biological realism, focused on explaining a few features of the collective behavior. Using tools related to nonlinear dynamics, such models come in various forms like traditional dynamical systems [17–19], continuous media [20–22], mean field approximations [23], maps [24,25]; models incorporating morphology and structure [26–31]; models with competition both at the network level [19] or at the synaptic level via plasticity [15] (see Chap. 1 for a survey). As usual, a trade-off is necessary to balance the level of detail and the scope of any attempt to come out with a useful model, i.e. to predict behavior or a particular trait accurately and reproducibly.

In [16], a thorough exposition of the basic mechanisms by which neuronal dynamical features can be understood is presented and the common idea of the existence of a threshold is challenged. In [32], a review of the state of affairs of neuronal network modeling surveying a wide range of techniques and information of the present state of phenomenological advances is available. The frontier between complex network structures and associated dynamics is extensively detailed in [33]. A bold perspective appearing in [34] argues that the level of knowledge of the biological intricacies of brain areas and layers has reached such a mature level that time is ripe to attempt a larger scale brain simulation of a microcolumn, calibrated to be indistinguishable from a real one.

The real lack of detailed knowledge of connectivities in the mammalian brain suggests that a wide range of possibilities should be tried when simulating networks of many neurons. This poses a computational challenge. The main goal of this chapter is to show the simulation work we produced during the Summer School using and modifying the code presented in Chap. 11 using the general scheme of Chap. 9 that tries to take on account neural structures and connectivities. It is important to remember that other efforts to simulate computationally large communities of neuronal cells have been done with different objectives in mind, for example [35,36] or the various references in [34]. Although interesting and efficient, those initiatives do not permit a straightforward extension to allow for structured areas with their natural connectivity patterns.

This chapter reports on a number of activities developed at the 5th summer school where we implemented a working framework for the simulation of large populations of neurons. Those neurons were treated as dynamical systems near a bifurcation so that variations of critical parameters would convert an otherwise quiescent state into a state of firing/bursting activity. Keeping track of all the information describing the network state in files would of course become prohibitive, so strategies for dealing with the data also were envisaged.

We chose the Morris-Lecar model as the unit in our simulations. This choice is based on the fact that its dynamics is well understood for the sake of the computational efficiency needed to produce data on a fine time scale and long simulation range. Its efficiency could be one order of magnitude better than the full Hodgkin-Huxley prototype neuron. Morris-Lecar is a conductance-based model like Hodgkin-Huxley but with only two persistent channels, one fast (Ca^{2+}) and one slow (K^{+}). Another group of participants dealing with the cat map (Chap. 13) implemented the Izhikevich model, see [17]. Any other dynamical model can be easily implemented as an additional module to the code (cf. Chap. 1).

The choice of the Morris-Lecar model could seem odd to a biologist, for this model was originally proposed to simulate features of a muscle cell, but the trade-off of biological realism for the possibilities of investigating a longer simulation and actually observing size dependent phenomena has paid off, especially when considering that many other biological facts were already left aside or oversimplified (e.g. synaptic dynamics, morphology, delay, etc.) for this particular set of studies. This is in full accordance with the original proposal of building a simple framework from scratch, avoiding black boxes, in a bid to better understand the role played by connectivity in large networked dynamical systems.

The idea of building a framework as general as we implemented is to start probing the functioning of the cat's brain. A vast amount of knowledge of its structures and connectivities has been collected during the last few years [37]. An important feature of the cat's brain is its subdivision into 53 functioning areas. The connection strength of these areas is assumed to be proportional to the thickness of nerves connecting them and is implemented in our code as well. One question that comes to mind is to what extent stimulating one area would spread activity to other areas. This main task is what we set about to address after polishing the code. Our results, while still too preliminary, look promising.

The chapter begins with a brief description, in Sect. 14.2, of the Morris-Lecar prototype neuron dynamics and its coupling to other neurons and the noisy environment. In Sect. 14.3, the idea of one neuronal area is developed and the conjecture of small world connectivity is implemented. This section also addresses the tuning of the network to a natural baseline behavior through parameter search. In Sect. 14.4, the procedure of tuning parameters to baseline behavior is re-introduced and preliminary results of our simulations, mainly the stimulation/ablation of areas and the effect of the size of the network, are

presented. Section 14.5 describes the relation of the known connectivity structure of cortex with the observed activity in the simulations. Last, Sect. 14.6 provides discussions on our results and poses important perspectives to be considered in the future using the general framework presented in Chap. 9.

14.2 The Model

14.2.1 The Morris-Lecar Neuron Model

The neuron model used in our simulations is the Morris-Lecar model. It is a simplified conductance model of the barnacle muscle fiber, with two variables obeying the equations:

$$\dot{v} = -g_{\mathrm{Ca}}(v)(v - V_{\mathrm{Ca}}) - g_{\mathrm{K}} w (v - V_{\mathrm{K}}) - g_L (v - V_L) + I_{\mathrm{ext}} \tag{14.1}$$

$$\dot{w} = \frac{\phi}{\tau_w(v)} (W_\infty(v) - w) \tag{14.2}$$

This is the dimensionless form of the model as presented by Rinzel and Ermentrout in their classic exposition [38]. Voltage v is normalized to the reversal potential of the excitatory ion Ca^{2+}, so voltage parameters are $V_{\mathrm{Ca}} = 1.0$, $V_{\mathrm{K}} = -0.7$ and $V_L = -0.5$. Conductances have been normalized by a reference conductance $G_{\mathrm{ref}} = 4\ \mathrm{mS/cm^2}$ and time by the time constant $\tau = C/G_{\mathrm{ref}} = 5$ ms, where $C = 20\ \mu\mathrm{F/cm^2}$. Thus we arrive at values $g_{\mathrm{K}} = 2.0$, $g_{\mathrm{Ca}} = 1.0$ and $g_L = 0.5$. In order to better match the model to the simulation of mammal cortex rhythms, one (dimensionless) time unit will henceforth be equivalent to 1 ms. Finally, $\phi = \frac{1.0}{3.0}$, and:

$$g_{\mathrm{Ca}}(v) = 0.5 \left[1 + \tanh \left(\frac{v + 0.01}{0.15} \right) \right] \tag{14.3}$$

$$\tau_w(v) = \frac{1}{\cosh \left(\frac{v - 0.1}{0.145} \right)} \tag{14.4}$$

$$W_\infty(v) = 0.5 \left[1 + \tanh \left(\frac{v - 0.1}{0.29} \right) \right] \tag{14.5}$$

This leaves the external current I_{ext} as the only free parameter. For low values ($I_{\mathrm{ext}} < I_{\mathrm{SN}}$), all orbits of the system are attracted to the unique stable node with most potassium channels closed and a low, polarized voltage (between V_L and V_{K}). As the external current grows beyond $I_{\mathrm{SN}} = 0.0833$, the stable node disappears via a saddle-node bifurcation in an invariant circle, giving way to an attracting limit cycle. In this cycle, the voltage jumps towards V_{Ca} and triggers the opening of potassium channels, which in turn pull the voltage back to polarized values; potassium channels then close and the cycle begins again. The result is rhythmic spiking beginning at infinitely low frequencies,

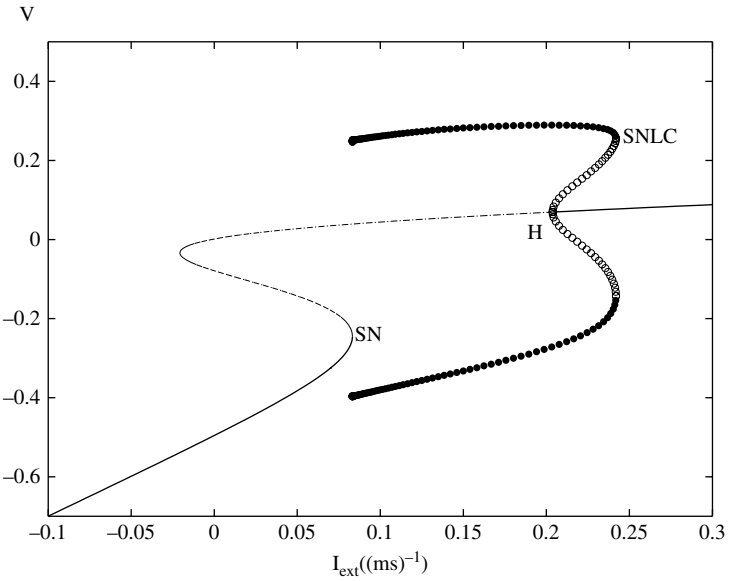

Fig. 14.1. Bifurcation diagram of the Morris-Lecar model used in this chapter. SN, saddle-node on invariant circle. H, Hopf. $SNLC$, saddle-node of limit cycles

and therefore, for the values of parameters chosen, Morris-Lecar is a class I model (for other choices of parameters, it may be a class II model ; see [38]).

Figure 14.1 completes the picture of bifurcations with external current. When $I_{\text{ext}} = I_{\text{SNLC}} = 0.242$, the limit cycle disappears through collision with an unstable limit cycle (born at a subcritical Hopf bifurcation of the hitherto unstable focus of the system) and the neuron becomes silent again, this time at a depolarized value of voltage. In this state, the external current is so strong that it effectively offsets the injection of potassium ions into the cell, preventing the firing of action potentials.

The parameter region of interest for our networks is the so-called excitable regime found at values of I_{ext} just below the threshold I_{SN} of rhythmic spiking. In this regime, if the voltage is pushed by the arrival of a synaptic impulse or by random noise out of equilibrium and across the unstable manifold of the saddle point, the system will make a long excursion in the phase plane, producing a single spike. This is illustrated in Fig. 14.2.

14.2.2 Coupling Between Neurons and External Stimulation

In the previous section, external current I_{ext} has been treated as a constant parameter. In network simulations, I_{ext} is a time-varying current coming from three sources:

$$I_{\text{ext}}(t) = I_{\text{bias}} + I_{\text{syn}}(t) + I_{\text{Poiss}}(t)$$

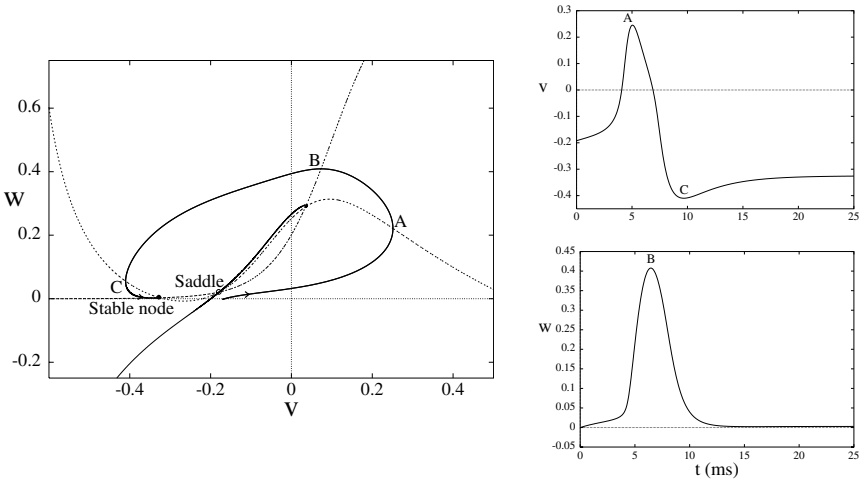

Fig. 14.2. Phase plane representation (**left**) and time evolution of variables v and w (**right**) for a single spike in the excitable regime ($I_{\text{ext}} = 0.07$) of the Morris-Lecar model. In the phase plane diagram, the thin continuous line is the unstable manifold of the saddle, dashed lines are the v and w nullclines, and the thick continuous line is the system trajectory. Point A, both in the phase plane and in the $v - t$ diagram, is the maximum of the action potential, where the trajectory crosses the v-nullcline. At point B, where the trajectory intersects the w-nullcline, there is maximal opening of potassium channels. Point C is the after-hyperpolarization peak due to remaining open potassium channels when the voltage first returns to the equilibrium level

- I_{bias} is a constant external bias current which will set the neurons in the excitable regime, as described in the previous section. It is common for all neurons.
- I_{syn} is the sum of synaptic currents arising from connections with other neurons in the network.
- I_{Poiss} also comes in the form of a synaptic current, but its origin lies outside the network; the presynaptic spikes that generate this current do not come from neurons in the network, but are instead randomly generated according to a Poisson process. These currents allow us to inject external stimulation.

We now describe the synaptic current $I_{\text{syn}}(t)$. It is a sum of currents due to both excitatory and inhibitory chemical synapses. Indeed, neurons in the network are classified as excitatory or inhibitory. If an excitatory presynaptic neuron fires at time t_{sp} (i.e. its voltage crosses zero with positive derivative), it adds to the term $I_{\text{syn}}(t)$ of the postsynaptic neurons an ohmic current $I_{\text{syn,exc}}(t)$ with reversal potential $V_{\text{exc}} = 0.05$ and time-varying, alpha function shaped conductance, thus:

$$I_{\text{syn,exc}}(t) = -g_{\text{exc}}\alpha_{\text{exc}}(t - t_{\text{sp}} - t_{\text{del}}) \cdot \Theta(t - t_{\text{sp}} - t_{\text{del}}) \cdot (v_{\text{post}}(t) - V_{\text{exc}}) \quad (14.6)$$

Here, g_{exc} is the strength of connection between pre- and postsynaptic neurons, t_{del} is the time delay of this connection, $\Theta(t)$ is the Heaviside step function, $v_{\text{post}}(t)$ is the postsynaptic neuron voltage and $\alpha_{\text{exc}}(t)$ is the alpha function:

$$\alpha_{\text{exc}}(t) = \frac{1}{\tau_{1,\text{exc}} - \tau_{2,\text{exc}}}(\mathrm{e}^{-\frac{t}{\tau_{1,\text{exc}}}} - \mathrm{e}^{-\frac{t}{\tau_{2,\text{exc}}}})$$

The smaller of the two time constants $\tau_{1,\text{exc}}$ and $\tau_{2,\text{exc}}$ is the rise time and the larger one is the decay time of the function. If, instead, the presynaptic neuron is inhibitory, the reversal potential is $V_{\text{inh}} = -0.50$ (i.e. equal to V_L) and the synaptic current added to $I_{\text{syn}}(t)$ is similarly:

$$I_{\text{syn,inh}}(t) = -g_{\text{inh}}\alpha_{\text{inh}}(t - t_{\text{sp}} - t_{\text{del}}) \cdot \Theta(t - t_{\text{sp}} - t_{\text{del}}) \cdot (v_{\text{post}}(t) - V_{\text{inh}}),$$

where $\alpha_{\text{inh}}(t)$ is now timed according to (possibly different) constants $\tau_{1,\text{inh}}$ and $\tau_{2,\text{inh}}$.

Finally, the $I_{\text{Poiss}}(t)$ term is very similar to $I_{\text{syn}}(t)$. The only difference is that it is made up exclusively of excitatory currents of the form of 14.6, and the times t_{sp} do not correspond to spikes of presynaptic neurons but are instead generated by a Poisson process. By varying the rate λ of this process, the amount of external stimulation injected into the different areas of our network may be chosen. Baseline values for non-stimulated areas are around $\lambda = 3$ Hz (mean period $T_{\text{Poiss}} = 333$ ms).

14.3 Setting Proper Parameters

The two-level network described in Chap. 9 gives rise to a moderately large number of parameters (connection numbers and strengths) that have to be tuned if we want our model to mimic cortex behavior. In this section, we describe the tuning procedure in two steps: first for intra-area parameters, and then for the whole 53 area network. Table 14.1 summarizes all the relevant parameters of the model and gives default values for them.

14.3.1 Optimal Inhibitory and Excitatory Coupling Strength for one area

In the absence of specific external stimulation, we would like neurons in our network to receive balanced excitatory and inhibitory input, so as to maintain a baseline activity corresponding to the non-specific Poissonian stimulation of 3 Hz. If this balance is achieved, scaling of connection strength with the square root of the degree (see Chap. 9) will ensure that input amplitude is independent of the number of neurons in the network (which is bounded by computational constraints). Balance of excitation and inhibition in one area depends on coupling parameters $g_{1,\text{inh}}$ and $g_{1,\text{exc}}$. In order to find appropriate values for these parameters, we did the following:

Table 14.1. Parameters of the network model and their default values grouped as: neuronal model parameters, network topology, connectivity strength and delays

Parameter	Description	Default value
I_{bias}	Constant bias current	0.08
V_{exc}	Reversal potential for excitatory synapses	0.05
V_{inh}	Reversal potential for inhibitory synapses	-0.5
n	neurons per area	512
p_{inh}	Ratio of inhibitory neurons	0.2
p_{ring}	Ratio of connections inside one area	0.1
p_{rew}	Probability of rewiring	0.3
p_3	Ratio of neurons receiving synapses from a connected area	0.05
p_4	Ratio of neurons with synapses towards a connected area	0.05
$g_{1,\text{exc}}$	Non-normalized strength of intra-area excitatory synapses	0.075
$g_{1,\text{inh}}$	Non-normalized strength of intra-area inhibitory synapses	2.5
$g_{2,\text{exc}}$	Non-normalized strength of inter-area excitatory synapses	0.075
$g_{2,\text{inh}}$	Non-normalized strength of inter-area inhibitory synapses	0
g_{ext}	Strength of connection for Poissonian currents	0.1
$\tau_{1,\text{exc}}, \tau_{2,\text{exc}}$	Rise and delay times of excitatory synaptic current	1 ms, 3 ms
$\tau_{1,\text{inh}}, \tau_{2,\text{inh}}$	Rise and delay times of inhibitory synaptic current	1 ms, 3 ms
$t_{\text{del},1,\text{exc}}$	Delay of intra-area excitatory synapses	1 ms
$t_{\text{del},1,\text{inh}}$	Delay of intra-area inhibitory synapses	3 ms
$t_{\text{del},2,\text{exc}}$	Delay of inter-area excitatory synapses	3 ms
$t_{\text{del},2,\text{inh}}$	Delay of inter-area inhibitory synapses	9 ms
T_{Poisson}	Mean period of Poisson excitation	333 ms

- In the absence of inhibition ($g_{1,\text{inh}} = 0$), we measured the mean firing rate (MFR) of the network (total number of spikes per second per neuron) as a function of the strength of excitatory synapses $g_{1,\text{exc}}$. Poissonian stimulation at a rate of 3 Hz is added to elicit baseline network activity. As is shown in Fig. 14.3(left), for $g_{1,\text{exc}} < 0.05$, the MFR is close to the externally imposed Poisson rate. At around $g_{1,\text{exc}} \approx 0.05$, activity blows up to a state of higher MFR where spiking is self-sustained and independent of the external input.
- Selecting a value for $g_{1,\text{exc}}$ barely above the threshold of sustained MFR ($g_{1,\text{exc}} = 0.075$), we increased the strength of inhibitory connections until the activity turned back to the background level as shown in

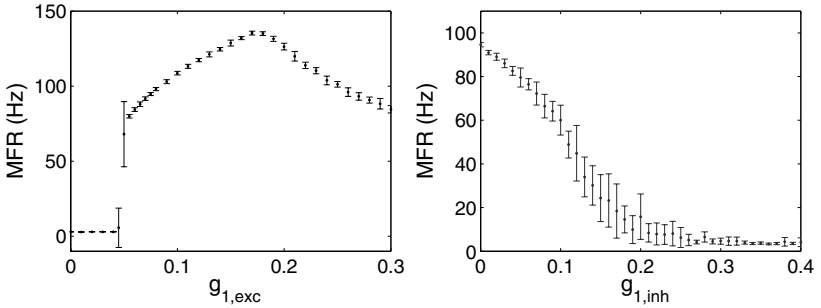

Fig. 14.3. (**Left**) Mean firing rate in one area of $n = 512$ neurons as a function of the strength of excitatory synapses for $g_{1,\mathrm{inh}} = 0$. Each point is an average of 25 simulations; (**Right**) Mean firing rate in one area of $n = 512$ neurons as a function of the strength of inhibitory synapses for $g_{1,\mathrm{exc}} = 0.075$. Each point is an average of 25 simulations

Fig. 14.3(right). At this point, excitatory and inhibitory forces within one area are balanced.

In order to check if both forces are balanced, we have measured the MFR as a function of the number of neurons n in one area for two sets of parameters. The first one corresponds to the pair ($g_{1,\mathrm{exc}} = 0.075$, $g_{1,\mathrm{inh}} = 0.25$), which produces a 3 Hz firing rate (see Fig. 14.3) and the second one, ($g_{1,\mathrm{exc}} = 0.075$, $g_{1,\mathrm{inh}} = 0.1$), is chosen such that there is more excitation than inhibition. This imbalance is going to be dependent on area size as shown in Fig. 14.4, while for the right selection of the excitatory and inhibitory strengths, the MFR remains constant at background level.

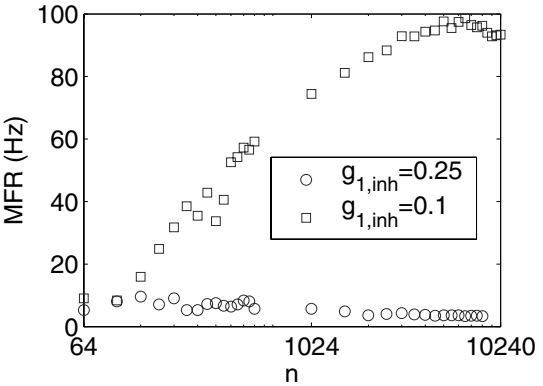

Fig. 14.4. Comparison of the MFR as a function of the number of neurons n per area between two sets of coupling strengths. When inhibition is not well balanced, the MFR increases as n becomes larger

14.3.2 Tuning Inter-area Parameters

When the 53 areas are coupled with the choice of parameters of the previous section, making $g_{2,\mathrm{exc}} = g_{1,\mathrm{exc}}$ and $g_{2,\mathrm{inh}} = 0$, a firing pattern that we will call "generic" was observed, see Fig. 14.5. All areas show a similar homogeneous pattern of activity, only the firing rate differs. Overexcitation can be determined to be responsible for this result. Therefore, a more extensive search for parameters that yielded spontaneous bursting (the desired physiologic phenomenon) was performed to elucidate suitable ranges and ratios of parameters in the model. In addition, trends were noted on how such parameters affect general behavior, including bursting, spike rates, and propagation through the systems of the simulated cortical structures.

Even though the parameter values chosen for a single area produced activity patterns and firing rates analogous to "natural" activity, the extension to 53 areas, through incorporation of the connectivity matrix, affected the behavior of each area. The primary effect was the introduction of additional activity in each area from all the areas that it is connected to with afferent connections. This extra activity increased the mean firing rate of each area to frequencies higher than desired, higher than the 10–40 Hz range. Since the parameters for excitatory and inhibitory connections within each area have the greatest influence on the mean firing rate, we performed simulations of the whole model with different combinations of these values. Figure 14.6 summarizes the results of all these simulations. From these plots, we chose the parameters $g_{1,\mathrm{inh}} = 0.4$ and $g_{2,\mathrm{exc}} = 0.075$ as the ones providing the most appropriate firing rates.

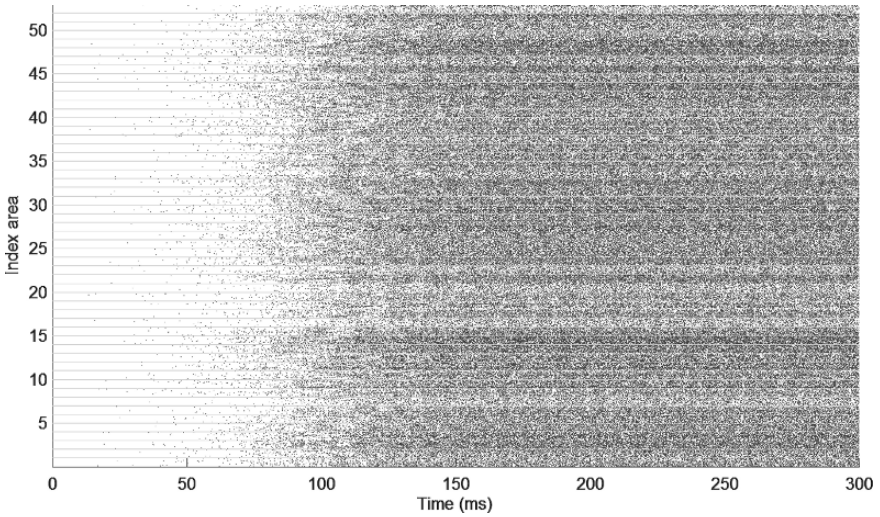

Fig. 14.5. Raster plot of the behavior of the whole cortex characterized as "generic". $g_{1,\mathrm{inh}} = 0.4$, $g_{2,\mathrm{inh}} = 0$, $g_{1,\mathrm{exc}} = g_{2,\mathrm{exc}} = 0.075$, $p_{\mathrm{ring}} = 0.05$, $p_{\mathrm{rew}} = 0.2$

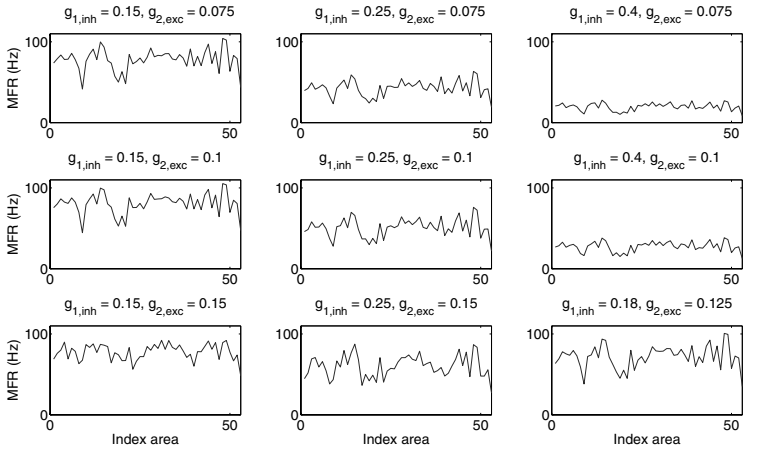

Fig. 14.6. Mean firing rate of each area, under nine different combinations of $g_{1,\mathrm{inh}}$ and $g_{2,\mathrm{exc}}$. $p_{\mathrm{ring}} = 0.05$, $p_{\mathrm{rew}} = 0.2$. Chosen parameters for further simulations: $g_{1,\mathrm{inh}} = 0.4$ and $g_{2,\mathrm{exc}} = 0.075$

Despite the fact that our model was now able to produce activity within the desired firing rate range, the overall behavior of areas continued to be rather homogeneous. We interpreted this result as not being "natural" behavior and called it "generic".

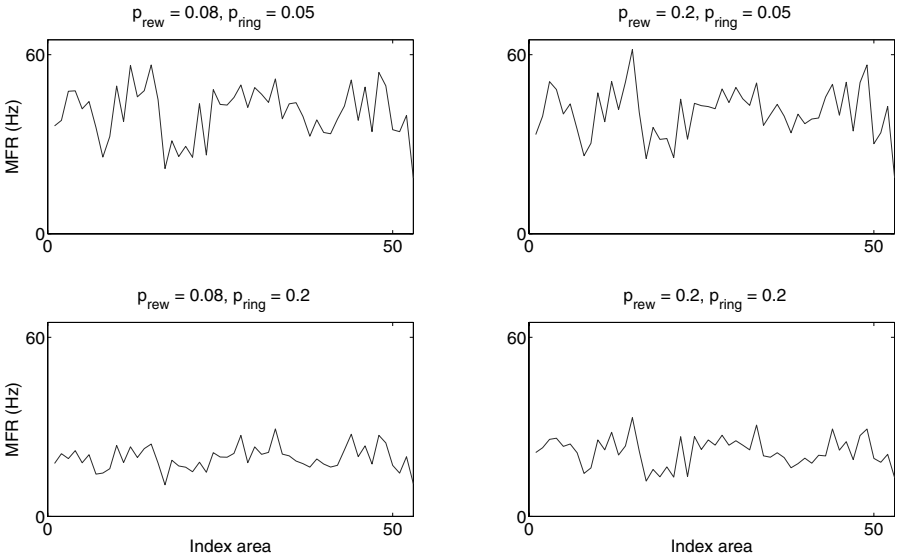

Fig. 14.7. Mean firing rate of each area, under four different combinations of p_{ring} and p_{rew}. Chosen parameters for later simulations: $p_{\mathrm{ring}} = p_{\mathrm{rew}} = 0.2$

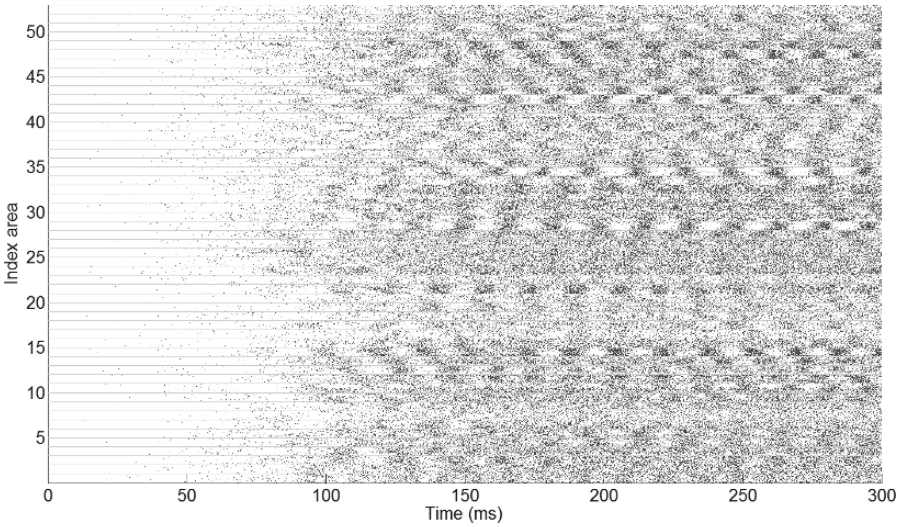

Fig. 14.8. Raster plot of the behavior of the whole cortex characterized as "natural". $g_{1,\text{inh}} = 0.4$, $g_{1,\text{exc}} = 0.075$, $p_{\text{ring}} = p_{\text{rew}} = 0.2$

Therefore, a set of further parameter search simulations were carried out where different combinations of the connectivity within each area were investigated, see Fig. 14.7. In this set of simulations, as before, our primary determining factor for "natural" behavior was to conserve the mean firing rate within the desired ranges. The additional condition was to obtain raster plots that presented different patterns of activity. Considering that the highest number of connections between areas is within each system, we desired that the areas of each system behave in a similar manner, and the behavioral pattern of each system be different from each other, hence representing each system's different function. This second condition was satisfied by setting parameters p_{ring} and p_{rew} to 0.2 (each area is modeled by a "small-world" subnetwork composed of 512 neurons. The number of connections is controlled by parameter p_{ring} and the deviation from the initial ring by p_{rew} (see Chaps. 3 and 9 for detailed descriptions)). Figure 14.8 presents the behavior obtained with these parameters.

14.4 Simulation of the Cat Cerebral Cortex

Once we managed to configure our model to behave in the manner of Fig. 14.8, we were more confident that the effects of the connectivity matrix were significant and that the behavior of the model could be described as "natural". We remind the reader that, as discussed in Chap. 3, the given corticocortical network has been found to be divided into four major clusters, corresponding to sensorial systems. Areas indexed 1–16 correspond to *visual cortex*, 17–23

represents the *auditory cortex*, indices 24–39 *somatosensory-motor cortex* and $40-53$ *frontolimbic* cortical areas. Next, we aimed to simulate different conditions of the neural network:

- The already achieved natural behavior, under the conditions of background noise (simulated by low frequency Poisson noise). Area coupling propels connected areas into correlated patterns of bursting, behavior remaining similar within each of the 4 cortical systems. Due to the small number of connections between systems, each system is to follow its own independent behavior.
- Stimulation of a single area, and of a whole system. From the sparseness of connection weights in the matrix beyond each system, and the existence of areas operating as "communication hubs", a preferential pathway of inter-system communication is implied. Stimulation of an area, or system, with a simulated external signal was expected to propagate to other systems of the network along this preferential pathway.
- The effects of ablating an area. The existence of only a small number of areas preferential for inter system communication implies a greater significance for these areas for network operation. Removal of these areas from the model should contribute to a great change of the overall activity of the network. To further confirm that our model was adequately representative of cat cerebral cortex and to observe the effects of the removal of such areas, we carried out simulations where such areas were ablated.

We thus proceeded to simulate stimulation of a part of the cortex to observe the propagation of the stimulation and the effects on the non-stimulated parts. Considering that the visual system is one of the most important, if not the primary, stimulus receiving part of the cortex, we simulated our model with stimulation of pulses at 25 Hz on the whole visual system. It is clear from Fig. 14.9, as expected, that the independent behavior of the other systems and areas of the cortex was dominated by the stimulation. Specifically, we can observe that the visual system transfers the introduced activity into the other systems and functions as the driving system for the whole cortex.

Our final simulations considered the effects of damaged tissue. To observe these effects, we simulated our model with stimulation and in addition, we inactivated areas that operated as midpoints in the pathway from the stimulation area to other areas. In these simulations, to represent area "death" or "ablation", we lowered the excitability parameter, I_{bias}, of the neurons within the target area slightly below their excitable regime. In addition, since the effects of stimulation of the whole visual cortex were so dominating that subtle changes of the network ("ablation" of an area) were not affecting the overall behavior, we limited ourselves to stimulating only "area 17" (*primary visual cortex*, index: 1) with pulses at 25 Hz. Areas "Ia", "35", and "36" (indexes: 43, 48 and 49; frontolimbic areas) were active (Fig. 14.10) or inactive (Fig. 14.11). Inactivation of these frontolimbic areas can be seen to

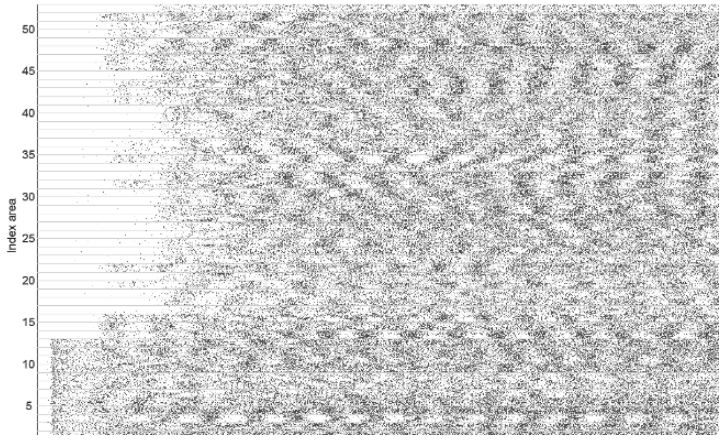

Fig. 14.9. Raster plot of the behavior of the whole cortex characterized under stimulation of the whole visual cortex

affect the auditory system (indices: 17–23) lowering its activity and synchronization as expected, since part of the functions of the limbic system is to connect the visual system with the auditory system.

Aside from configuring and simulating our model to observe the above behaviors, we also attempted a simulation with a large number of neurons ($> 10^6$). This was done mostly as a computational task and the parameters for this simulation were not in accordance to the other simulations. Regardless, the behavior exhibited by our model with this large number of neurons is

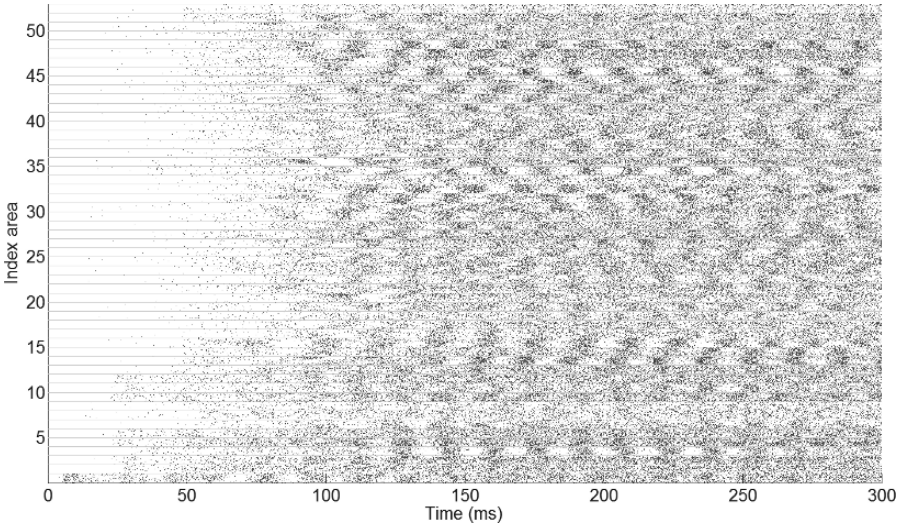

Fig. 14.10. Raster plot of stimulation of area "17" (primary visual cortex, index: 0)

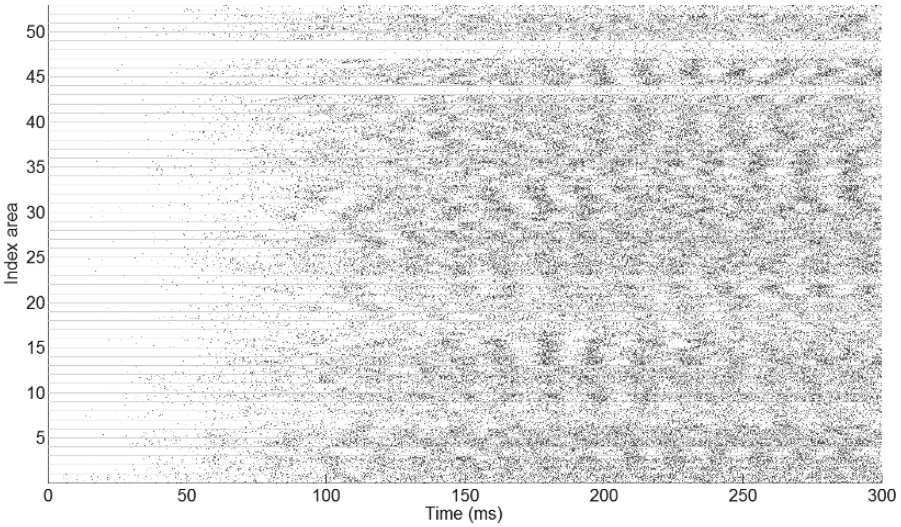

Fig. 14.11. Stimulation of area "17", while areas "LA", "35", and "36" (indices: 43, 48 and 49; frontolimbic cortex) are inactive

presented in Fig. 14.12. Considering that the parameters were different from our other simulations, the result is obviously misleading. We believe the strong oscillatory pattern observed to be related to the dynamics of the Morris-Lecar neuronal model. Looking at its bifurcation diagram, shown in Fig. 14.1, we argue that for the given parameters, all neurons must have collectively followed similar changes in their dynamical states. When so many neurons are present

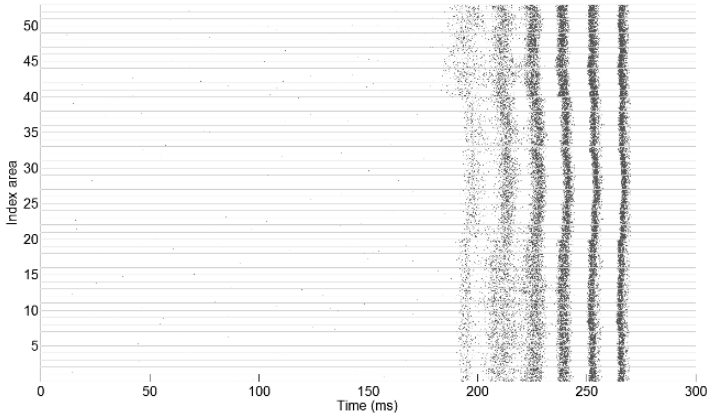

Fig. 14.12. Raster plot of the behavior of a cortex of $1,085,440$ neurons, which corresponds to $20,480$ neurons per area. $g_{1,\mathrm{inh}} = 0.4$, $g_{1,\mathrm{exc}} = 0.075$, $g_{2,\mathrm{exc}} = 0.15$, $p_{\mathrm{ring}} = 0.05$, $p_{\mathrm{rew}} = 0.1$

within each cortical area, each neuron receives an extremely large amount of input, which, after a brief period of intense firing, raises their I_{bias} triggering all neurons beyond the *SNLC* point into the "silent regime". Once all neurons are silent, only noise is present in the system, allowing neurons to recover their "excitatory state" and start firing again after a brief pause. Unfortunately, we could not perform further simulations of this size due to computer time limitations.

14.5 Dependence of MFR on Anatomical Connectivity

In this section, we present a brief attempt to explore the relationship between the observed behavior of the simulated system and the structural properties of the network. We will look for correlations between the characteristic firing rate of each cortical area obtained in the simulations with its degree and intensity. We will also try to find a simple analytical solution to explain the observed dynamics.

In Sect. 14.4, firing rates of individual cortical areas were estimated from the simulations. Frequency is observed to be modulated within about 10–20 ms (look at the fine structure of Fig. 14.8). On the other hand, under stationary conditions it varies significantly from area to area (Fig. 14.13). The variation of $g_{2,\text{exc}}$ (inter-areal excitatory coupling strength) and $g_{1,\text{inh}}$ (intra-areal inhibitory coupling strength) contributes to the absolute value of the mean firing rate. In the chosen parameter range, $g_{2,\text{exc}} \in [0.075, 0.15]$ and

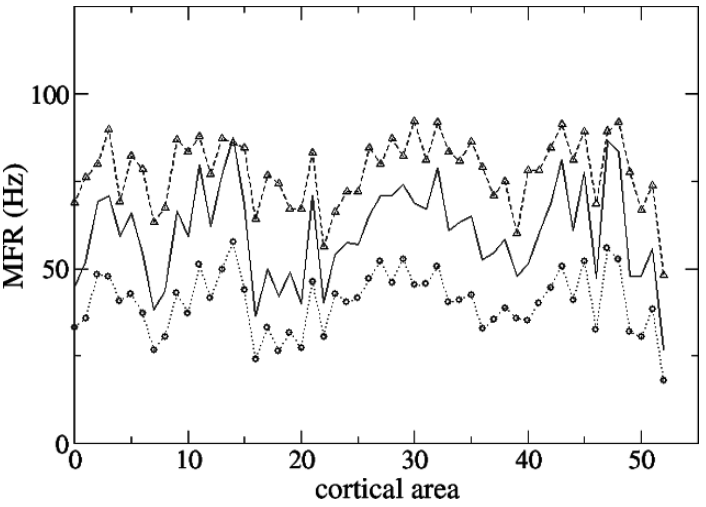

Fig. 14.13. Dependence of the firing rate on the internal and external coupling strength. $g_{2,\text{exc}} = 0.15$ in all cases. Dashed line: $g_{1,\text{inh}} = 0.15$, solid: $g_{1,\text{inh}} = 0.25$, dotted: $g_{1,\text{inh}} = 0.4$

$g_{1,\text{inh}} \in [0.15, 0.4]$, the mean firing rate of the areas was found to lie between 25 to 100 Hz. The main curve profile remains unchanged for different values of $g_{1,\text{inh}}$ and $g_{2,\text{exc}}$. Modification of the $g_{1,\text{inh}}$ coupling shifts the curve in the vertical direction, i.e. higher frequencies are achieved with lower inhibition. This fact indicates the importance of inhibitory connections in the modulation of brain dynamics. Indeed, inhibitory coupling has been shown to suppress oscillations induced by the excitatory coupling as is known to happen in pathology such as epileptic seizures caused by excessive synchronization of neuronal activity [39].

14.5.1 Correlation to k^{in} and S^{in}

The input degree of a node k^{in} refers to the number of connections a node receives. Its natural extension for weighted networks, the input intensity of a node S^{in}, is the sum of the strength of its input connections. Although there are many existing network measures (see Chap. 3 for descriptions of network characterization and properties of the cat cortex), here, we will only explore the relationship between the mean firing rate and k^{in} and S^{in}.

The average response of a cortical area depends directly on the amount of input signal received, thus we will correlate the MFR to k^{in} and S^{in} of the cortical areas. Linear correlation of both measures with the MFR obtained from simulations is depicted on Fig. 14.14. As expected, it is a monotonously increasing function of k^{in} and S^{in}. The more input a cortical area receives, the more often its neurons will fire. The linear fit is better in the case of intensity, since the relation between the MFR and k^{in} slightly saturates at high degrees ($k^{\text{in}} \geq 20$). This saturation is more pronounced in other parameter sets (not shown). Figure 14.17 shows that correlation between the MFR and S^{in} is higher for most of the parameter sets.

14.5.2 Analytical Estimation

In the following, our modest effort to model the observed MFRs for each cortical area is presented. A commonly used approach in artificial neural networks

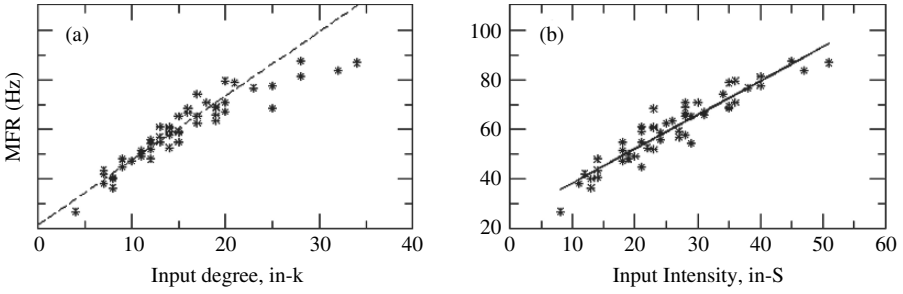

Fig. 14.14. Correlation of average simulated Mean Firing Rates per area (MFR) with: (**a**) degree and; (**b**) intensity

is to define an activation function describing the average response of neurons to input received from its neighbors. In a general form, the equations are written as:

$$r_i(t+1) = F(h_i)$$
$$h_i = a\sum_{j=1}^{N} W_{ij} r_j(t) + \xi, \quad i = 1, ..., N,$$

r_i being the activity of the neuron, W_{ij} the weighted adjacency matrix of the network and ξ some external input, i.e. noise. $F(h_i)$ is usually some sigmoidal saturation function and is normalized either to $[0, 1]$ or $[-1, 1]$. Parameter a controls the slope of the saturation function tuning the scale of the response. Such a function sums up all inputs the neuron receives and returns a normalized output representing its average activity response.

Similar approaches have already been used for cortical models of the cat [40, 41]. Here, we simulate cortical areas instead of individual neurons. This approach is reasonable since the mean activation level of a cortical area strongly depends on the amount of input received from its neighbors in a cumulative and smooth manner, which could be highly arguable in the case of individual neurons [42, 43]. As said above, the number of firing neurons scales with the input an area receives. Here, mean activity level will be considered to be equivalent to MFR. The simplest choice is to assume a linear approximation

$$F(h_i) = \alpha h_i + \beta, \text{ where } \beta = 0$$

(the saturation function crosses the origin). Our study is then limited to estimating the slope parameter a and noise level ξ to provide an optimal approximation to the results obtained from the simulations.

In the steady state $r_i(t+1) = r_i(t)$ and after taking $F(h_i)$ to be linear, equations reduce to:

$$r_i = \alpha \left(a\sum_{j}^{N} W_{ij} r_j + \xi \right).$$

After rescaling, we arrive at the following equation in matrix form:

$$\boldsymbol{r'} = (\boldsymbol{I} - a'\boldsymbol{W})^{-1}\,\boldsymbol{\xi'}, \tag{14.7}$$

where $\boldsymbol{r'}$ is the MFR vector of the 53 areas, $\boldsymbol{I}$ is the identity matrix, $\boldsymbol{W}$ is the adjacency matrix of the cortical network, $a' = \alpha a$, and $\boldsymbol{\xi'}$ is a column vector where all elements are $\alpha\xi$.

Our main purpose is to find the coupling strengths $g_{1,\text{inh}}$ and $g_{1,\text{exc}}$ that produce estimated MFRs as closely correlated to the MFRs from our simulations as possible. We face the problem of setting both slope a' and noise

ξ' parameters satisfactorily. There is a limited range of a's we can examine because the maximum eigenvalue of our dynamical system (given by the adjacency matrix $\boldsymbol{W}$) is $\lambda_{\max} = 29.08$, and thus $a' \approx 1/\lambda_{\max} = 0.034385$. At this value, the system has a singularity and solutions with larger a' are unstable. Correlation is "blind" to this singularity, and thus, in order to look for proper a' and ξ', we will calculate the Euclidean distance between the estimated $\boldsymbol{r'}$ vectors and the vectors of MFRs for different $g_{1,\text{inh}}$ and $g_{2,\text{exc}}$ obtained from our simulations. Figure 14.15a shows how estimated MFRs differ from simulated MFRs for different values of a'. In this representation, the singularity is clearly observed as the distance between $\boldsymbol{r'}$ and MFR vectors grows to infinity (Fig. 14.15b).

Importantly, Fig. 14.15(b) also shows the presence of a minimal distance, so in the following, our optimization problem is to find the closest $\boldsymbol{r'}$ solutions to the MFR from simulations. Among the stable solutions ($a' < 0.034385$), the shortest distance depends both on a' and ξ' for each coupling strength combination. After solving (14.7) for different parameters a' and ξ', optimal values were found for each combination of $g_{1,\text{inh}}$ and $g_{2,\text{exc}}$ as summarized in Table 14.2.

We are now ready to look for the optimal coupling strengths. For each pair of $g_{1,\text{inh}}$ and $g_{2,\text{exc}}$, the simulated MFRs and the vector $\boldsymbol{r'}$ estimated for corresponding optimal a' and ξ' (see Table 14.2) are correlated. Results are shown in Fig. 14.16. Note that the best correlation is for the values of the coupling parameters that produce lower MFRs. Interestingly, the properly balanced inhibitory coupling allows us to achieve both "natural behavior" and maximal correlation to the linear approximation. Too low as well as too high inhibition gives rise to a marked decrease of this correlation for all excitatory values.

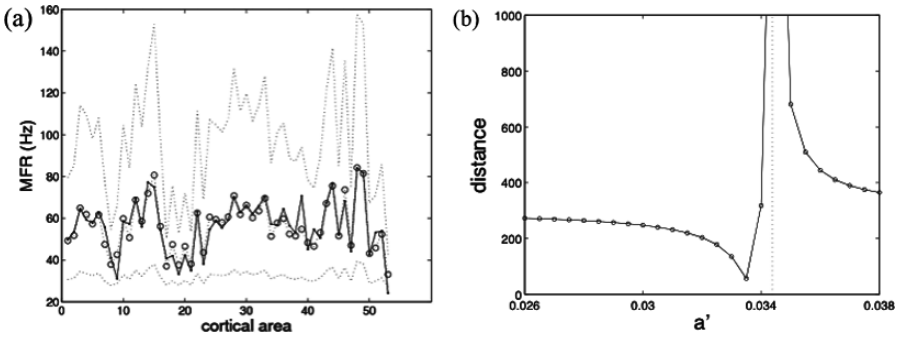

Fig. 14.15. **a**) Simulated MFR of the 53 cortical areas (*solid*) and estimated MFRs with $\xi = 24.5$ and different a' values (*dotted lines*). Distance between simulated and estimated MFRs varies significantly for different parameters; **b**) Setting $\xi' = 1.0$, the singularity of the dynamical system appears as distance going to infinity at $a' = 0.034385$. Larger values of a' represent unstable solutions

Table 14.2. Optimal values of slope a' and noise ξ' for different coupling strengths

$g_{2,\mathrm{exc}}$	$g_{1,\mathrm{inh}}$	opt a'	opt ξ'	$g_{2,\mathrm{exc}}$	$g_{1,\mathrm{inh}}$	opt a'	opt ξ'
0.075	0.15	0.0145	47.0	0.125	0.15	0.0135	50.0
	0.18	0.0175	33.5		0.18	0.0175	37.5
	0.2	0.0185	28.0		0.2	0.0190	32.0
	0.25	0.0200	19.0		0.25	0.0205	24.5
	0.3	0.0200	14.5		0.3	0.0210	20.0
	0.4	0.0195	9.0		0.4	0.0195	16.0
0.1	0.15	0.0140	50.0	0.15	0.15	0.0130	50.0
	0.18	0.0175	36.0		0.18	0.0165	39.5
	0.2	0.0190	30.0		0.2	0.0190	32.5
	0.25	0.0205	22.0		0.25	0.0220	23.5
	0.3	0.0200	18.5		0.3	0.0215	21.5
	0.4	0.0210	11.5		0.4	0.0205	17.5

Increasing the excitatory coupling $g_{2,\mathrm{exc}}$ produces, in general, a monotonous increase of correlation.

Finally, we compare the results from this analytical linear estimation to the effects of degree and intensity distribution. Vectors of input degrees k^{in} and input intensities S^{in} of cortical areas are correlated to the MFRs from the simulation as shown in Fig. 14.17. As expected from the weighted nature of the adjacency matrix, intensities do correlate better than degrees. After all the optimization effort, high correlation values suggest that our model behaves as a linear system for a certain range of coupling strengths (see Fig. 14.17). This is also supported by the high correlation between simulated MFRs and intensities S^{in}. Indeed, the analytical estimations show only slightly better correlation than the S^{in}.

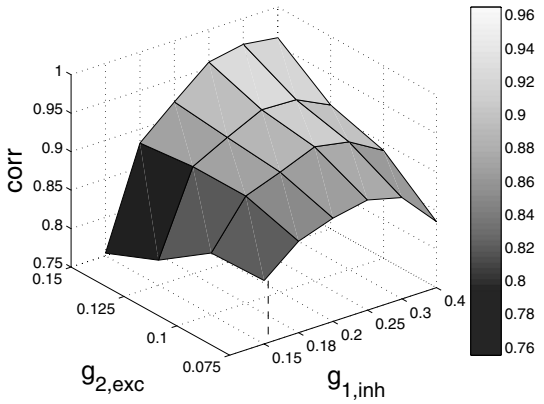

Fig. 14.16. Correlation between MFR from simulations and estimated $\boldsymbol{r'}$ using optimal a' and ξ' for each set of $g_{1,\mathrm{inh}}$ and $g_{2,\mathrm{exc}}$

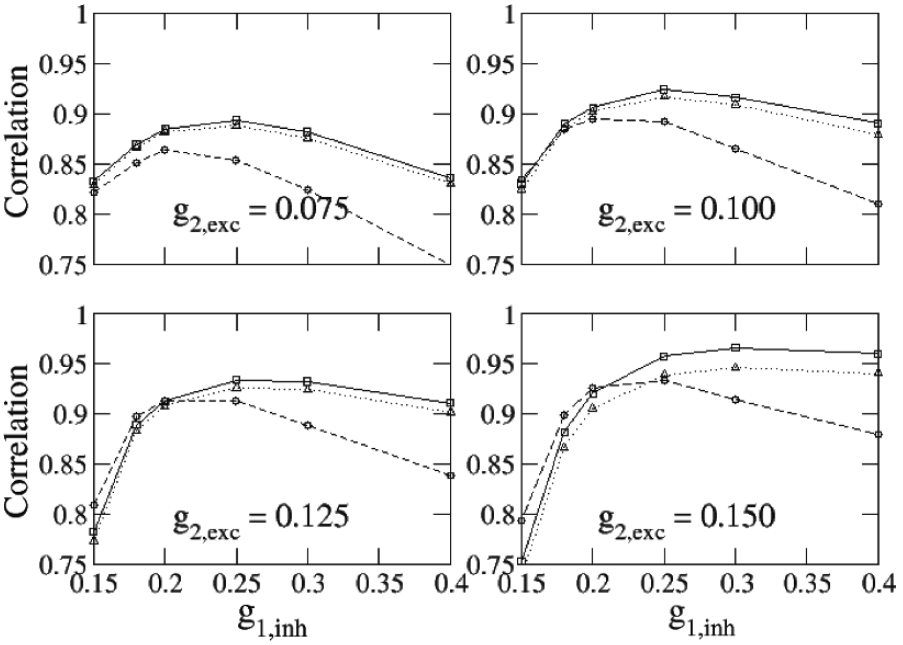

Fig. 14.17. Comparison of the correlation between computed MFR and estimated MFR at parameter a' (*solid line*), degree (*dashed*), intensity (*dotted*)

14.6 Conclusions and Outlook

During this set of computational exercises, we learned principles of large-scale neuronal simulations using the parallel code initially given to us. We defined a method to look for parameters that would provide a *realistic behavior*. We observed that finding suitable parameters and obtaining robust behavior is difficult. First, for the internal sub-network representing each cortical area, a set of excitatory/inhibitory strengths was found that would provide stable response with increasing size of the sub-network (see Fig. 14.4). The requirement was to keep average firing rate of individual neurons around 3 Hz. Then, after connecting the 53 subnetworks and assuming equal $g_{1,\mathrm{exc}}$ and $g_{2,\mathrm{exc}}$, the network showed too high a MFR, which was re-balanced by increasing the strength of inhibitory connections (Fig. 14.7). But this change happened to break the balance again as seen in the simulation with a million neurons, where the effect of scaling is evident.

However, raster plots displayed rather homogeneous and similar behavior of all cortical areas (Fig. 14.5), a behavior we called "generic". Looking for different, more realistic behaviors, we performed a parameter search on p_{ring}

and p_{rew} in order to change the network structure and hopefully also the behavior. A regime in which cortical areas exhibit bursting and silent epochs was found providing more interesting dynamics that we called "natural behavior" (see Fig. 14.8).

Finally, as discussed in Sect. 14.5, our analytical estimations show that the model behaves on average as a linear network model where, apart from the bursting dynamics, the MFR of each cortical area is highly proportional to the total input received (see Fig. 14.14).

Several open questions remain and a large set of possible implementations can be tried out:

First, we are aware of the arbitrary manner in which "natural behavior" was characterized: based exclusively on keeping the MFR at biologically reliable levels observed experimentally and on visual inspection of raster plots to avoid homogeneous dynamical responses. Thus, more convenient methodology founded on different measures would be desirable in order to characterize and classify the observed dynamics. Such measures could depend on, e.g., temporal correlations, frequency content, information transfer, etc.

Second, in our simulations, the small-world network topology following the Watts-Strogatz model was used for the internal neural connections within one cortical area. This topology has already been shown to enhance signal propagation and network synchronization which are so important for exchange of information.

It would be desirable, however, to introduce more realistic internal connectivities modeling finer cortical structures like layers, columns and if possible, the morphology of cortical neurons. Current sparse knowledge of detailed connectivity at the neuronal level makes such an implementation improbable in the nearest future. An intermediate solution might rely on taking just a small set of cat's cortical neurons, extracting their approximate local topology and randomly replicating it in order to mimic the internal structure of a cortical area. On the other hand, representing cortical layers and all the available experimental data about their interconnectivity offers an interesting opportunity to improve the internal architecture of the model. A first initial step should be the modeling of hierarchical organization of the cortex introducing hierarchical subnetworks for each cortical area rather than the small-worlds used here.

And finally, the linear behavior described by the model is not expected in real brains. As a complex system per excellence, the brain does not perform only such trivial behavior. Further modifications might include the introduction of delays and improved simulation strategies to limit the continuous spread of activity typical of pathological situations. For future work, we should remark that the dependence of the mean firing rates on the intra-areal connectivity among neurons is yet to be tested. Observing and characterizing brain activity under external stimuli is also of high interest.

References

1. W. S. Armbruster, Evolution of floral form: electrostatic forces, pollination, and adaptive compromise, New Phytol., 152(2):181–183, 2001.
2. M. Golubitsky, I. Stewart, P.-L. Buono and J. J. Collins, A modular network for legged locomotion, Physica D, 115(1):56–72, 1998.
3. M. Golubitsky, M. Pivato and I. Stewart, Interior symmetry and local bifurcation in coupled cell networks, Dyn. Sys., 19(4):389–407, 2004.
4. H. Levine and E. Ben-Jacob, Physical schemata underlying biological pattern formation—examples, issues and strategies, Phys. Biol., 1:14–22, 2004.
5. S. Douady and Y. Couder, Phyllotaxis as a physical self-organized growth process, Phys. Rev. Lett., 68(13):2098–2101, 1992.
6. V. M. Eguíluz, M. Ospeck, Y. Choe, A. J. Hudspeth and M. O. Magnasco, Essential nonlinearities in hearing, Phys. Rev. Lett., 84(22):5232–5235, 2000.
7. P. Martin and A. J. Hudspeth, Compressive nonlinearity in the hair bundle's active response to mechanical stimulation, Proc. Natl. Acad. Sci. USA, 98(25):14386–14391, 2001.
8. PhysicsWeb, Best of physicsweb, Best of Physics in Biology, http://physicsweb.org/bestof/biology, 2006.
9. C. Koch and I. Segev, The role of single neurons in information processing, Nat. Neurosci., 3:1171–1177, 2000.
10. B. J. O'Brien, T. Isayama, R. Richardson and D. H. Berson, Intrinsic physiological properties of cat retinal ganglion cells, J. Physiol., 538(3):787–802, 2002.
11. R. H. Masland, The fundamental plan of the retina, Nat. Neurosci., 4(9): 877–886, 2001.
12. C. F. Stevens, Models are common; good theories are scarce, Nat. Neurosci., 3:1177, 2000.
13. L. C. Jia, M. Sano, P.-Y. Lai and C. K. Chan, Connectivities and synchronous firing in cortical neuronal networks, Phys. Rev. Lett., 93:088101, 2004.
14. J. van Pelt, I. Vajda, P. S. Wolters, M. A. Corner, W. L. C. Rutten and G. J. A. Ramakers, Dynamics and plasticity in developing neuronal networks in vitro, Prog. Brain Res., 147:173–188, 2005.
15. A. Van Ooyen, Competition in neurite outgrowth and the development of nerve connections, Prog. Brain Res., 147:81–99, 2005.
16. E. M. Izhikevich, Dynamical systems in neuroscience: the geometry of excitability and bursting, MIT Press, 2007.
17. E. M. Izhikevich, Which model to use for cortical spiking neurons, IEEE Trans. Neural Netw., 15(5):1063–1070, 2004.
18. R. C. Elson, A. I. Selverston, R. Huerta, N. F. Rulkov, M. I. Rabinovich and H. D. I. Abarbanel, Synchronous behaviour of two coupled biological neurons, Phys. Rev. Lett., 81(25):5692–5695, 1998.
19. M. Rabinovich, A. Volkovskii, P. Lecanda, R. Huerta, H. D. I. Abarbanel and G. Laurent, Dynamical encoding by networks of competing neuron groups: winnerless competition, Phys. Rev. Lett., 87(6):068102, 2001.
20. C. J. Rennie, P. A. Robinson and J. J. Wright, Unified neruophysical model of EEG spectra and evoked potentials, Biol. Cybern., 86:457–471, 2002.
21. J. J. Wright, C. J. Rennie, G. J. Lees, P. A. Robinson, P. D. Bourke, C. L. Chapman, E. Gordon and D. L. Rowe, Simulated electrocortical activity at microscopic, macroscopic and global scales, Neuropsychopharmacology, 28: 80–93, 2003.

22. P. A. Robinson, C. J. Rennie, D. L. Rowe, S. C. O'Connor, J. J. Wright, E. Gordon and R. W. Whitehouse, Neurophysical modeling of brain dynamics, Neuropsychopharmacology, 28:74–79, 2003.
23. H. R. Wilson and J. D. Cowan, A mathematical theory of the functional dynamics of cortical and thalamic neuron tissue, Kybernetik, 13:55–80, 1973.
24. M. Bazhenov, N. F. Rulkov, J.-M. Fellous and I. Timofeev, Role of network dynamics in shaping spike timing reliability, Phys. Rev. E, 72:041903, 2005.
25. G. Tanaka, B. Ibarz, M. A. F. Sanjuan and K. Aihara, Synchronization and propagation of bursts in networks of coupled map neurons, Chaos, 16:013113, 2006.
26. G. A. Ascoli, Progress and perspectives in computational neuroanatomy, Anat. Rec. (New Anat.), 257(6):195–207, 1999.
27. P. C. Bressloff, Resonantlike synchronization and bursting in a model of pulse-coupled neurons with active dendrites, J. Comput. Neurosci., 6:237–249, 1999.
28. S. M. Korogod, I. B. Kulagina, V. I. Kukushka, P. Gogan and S. Tyc-Dumont, Spatial reconfiguration of charge transfer effectiveness in active bistable dendritic arborizations, Eur. J. Neurosci; 16:2260–2270, 2002.
29. P. C. Bressloff and S. Coombes, Synchrony in an array of integrate-and-fire neurons with dendritic structure, Phys. Rev. Lett., 78(24):4665–4668, 1997.
30. L. da F. Costa, Morphological complex networks: can individual morphology determine the general connectivity and dynamics of networks?, oai:arXiv.org:q-bio/0503041, 2005.
31. L. F. Lago-Fernández, R. Huerta, F. Corbacho and J. A. Sigüenza, Fast response and temporal coherent oscillations in small-world networks, Phys. Rev. Lett., 84(12):2758–2761, 2000.
32. M. I. Rabinovich, P. Varona, A. I. Selverston and H. D. I. Abarbanel, Dynamical principles in neuroscience, Rev. Mod. Phys., 78:1213–1265, 2006.
33. S. Boccaletti, V. Latora, Y. Moreno, M. Chavez and D.-U. Hwang, Complex networks: structure and dynamics, Phys. Rep., 424:175–308, 2006.
34. H. Markram, The blue brain project, Nat. Rev. Neurosci., 7:153–160, 2006.
35. R. D. Traub and R. K. Wong, Cellular mechanism of neuronal synchronization in epilepsy, Science, 216:745–747, 1982.
36. A. Morrison, C. Mehring, T. Geisel, A. Aertsen and M. Diesmann, Advancing the boundaries of high-connectivity network simulation with distributed computing, Neural Comput., 17:1776–1801, 2005.
37. J. W. Scannell, G. A. P. C. Burns, C. C. Hilgetag, M. A. O'Neill and M. P. Young, The connectional organization of the cortico-thalamic system of the cat, Cereb. Cortex, 9:277–299, 1999.
38. J. Rinzel and G. B. Ermentrout, Analysis of neural excitability and oscillations, in Methods in neuronal modeling: from synapses to networks, ed. C. Koch and I. Segev, 135–169, MIT Press, Cambridge, MA, 1989.
39. P. Kudela, P. J. Franaszczuk and G. K. Bergey, Changing excitation and inhibition in simulated neural networks: effects on induced bursting behavior, Biol. Cybern., 88:276–285, 2003.
40. R. Kötter and F. T. Sommer, Global relationship between anatomical connectivity and activity propagation in the cerebral cortex, Phil. Trans. R. Soc. Lond. B, 355:127–134, 2000.
41. M. P. Young, C. C. Hilgetag and J. W. Scannell, On imputing function to structure from the behavioural effects of brain lesions, Phil. Trans. R. Soc. Lond. B, 355:147–161, 2000.

42. W. J. Freeman, Tutorial on neurobiology: From single neurons to brain chaos, Int. J. Bifurcation Chaos, 2(3):451–482, 1992.
43. P. beim Graben and J. Kurths, Simulating global properties of electroencephalograms with minimal random neural networks, Neurocomputing, doi: 10.1016/j.neucom.2007.02.007, 2007.